IEEE Photonics Journal
An IEEE Photonics Society Publication

Open Access

Switchable Generation of Multipulse Patterns of Noise-Like Pulse and Dissipative Soliton Resonance in a Fiber Laser

Volume 11, Number 5, October 2019

He Xu
Sheng-Ping Chen
Yue Tao
Zong-Fu Jiang

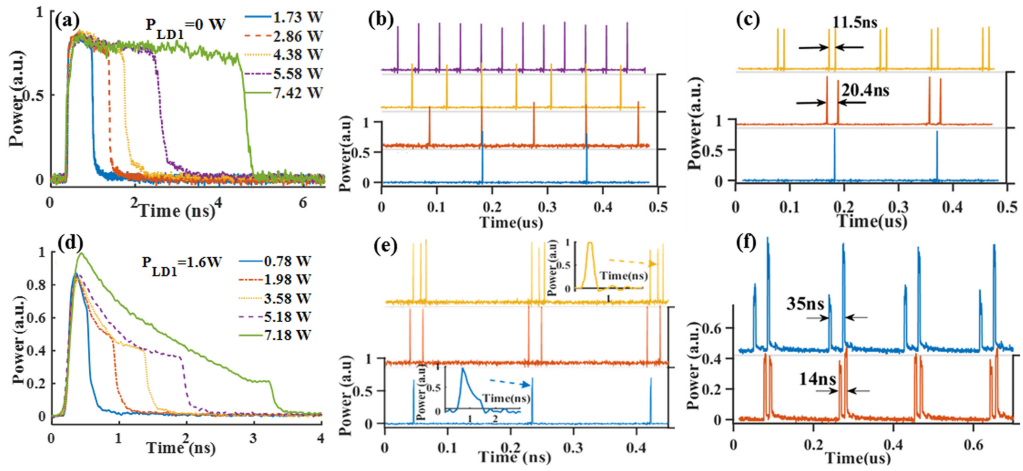

DOI: 10.1109/JPHOT.2019.2941283

Switchable Generation of Multipulse Patterns of Noise-Like Pulse and Dissipative Soliton Resonance in a Fiber Laser

He Xu,[1] **Sheng-Ping Chen**,[1,2,3] **Yue Tao**,[1] **and Zong-Fu Jiang**[1,2,3]

[1]College of Advanced Interdisciplinary Studies, National University of Defense Technology, Changsha 410073, China
[2]State Key Laboratory of Pulsed Power Laser Technology, Changsha 410073, China
[3]Hunan Provincial Key Laboratory of High Energy Laser Technology, Changsha 410073, China

DOI:10.1109/JPHOT.2019.2941283

Manuscript received June 28, 2019; revised August 24, 2019; accepted September 10, 2019. Date of publication September 13, 2019; date of current version October 4, 2019. This work was supported in part by National Natural Science Foundation of China (NSFC) under Grant 61235008 and in part by National High Technology Research and Development Program of China (2015AA021101). Corresponding author: Sheng-Ping Chen (e-mail: chespn@163.com).

Abstract: We report on the switchable generation of versatile patterns of multiple noise-like pulse (NLP) and dissipative soliton resonance (DSR) pulses in a dual-pump figure-eight mode-locked fiber laser. Benefiting from the change of saturation power influenced by pump power intercoupling, harmonic DSR pulses, dual-pulse DSR, dual-pulse and tri-pulse NLP are formed depending on different pump power combinations and intra-cavity polarization states. We find that the NLP pulse profile can turn from h-shape to triangular-shape after splitting. The dual-wavelength spectrum of the pulse, consisting of an obvious stokes line, can tune its center from 1075 to 1097 nm. This type of fiber laser may be helpful for further in-depth study on the underlying dynamics of multiple NLP and DSR pulses.

Index Terms: Fiber lasers, mode-locked lasers.

1. Introduction

High energy rectangular-shaped pulses in nanosecond time scales have attracted considerable attention due to their potential applications, including all-optical square-wave clocks, laser micromachining, range finding, and optical sensing [1], [2]. Dissipative soliton resonance (DSR) and noise like pulse (NLP) are two main kinds of rectangular-shaped pulses [3]–[5]. They both have the characteristics of pump-dependent pulse duration and peak power clamping (PPC) effect [6]. The difference is that DSR has no internal fine structures within the square profile packet, and therefore they maintain the pulse-to-pulse coherence. Though the NLP appears as a single pulse on the oscilloscope, it is a wave packet consisting of many ultrashort subpulses with certain clamped peak powers [7].

Though the DSR and NLP pulses are supposed to be breaking free with high pulse energy, they would break into multipulses under specific cavity parameters such as large dispersion [8], high nonlinearity [9] and high birefringence [10]. It is speculated that the initial number of multiple dissipative solitons (DSs) depends the number of DSRs because DSR never split [11], [12]. The

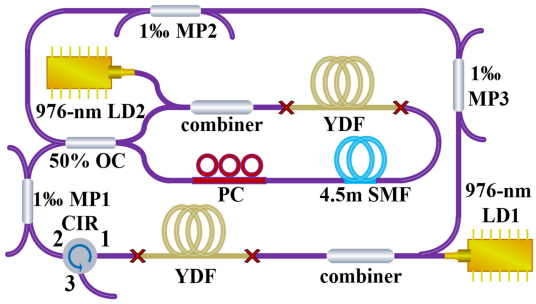

Fig. 1. Schematic configuration of the peak power tunable DSR laser. YDF: Yb-doped double-clad fiber; MP: monitor port; LD: laser diode; PC: polarization controller; OC: output coupler; CIR: circular.

reported multiple DSRs are all the same in amplitude, width and pulse intervals [13]. NLPs are able to break into various patterns involving non-uniform duration and spacing [14], [15]. Though generation of rectangular NLP and DSR in a fiber laser was reported [7], no pulse breaking phenomenon of the NLP and DSR simultaneously in one laser had appeared before.

In this paper, we report switchable generation of multi-pulse patterns of NLPs and DSRs in one cavity configuration consisting of two pumps with a nonlinear amplifying loop mirror (NALM). Plenty of studies based on the figure-eight NALM to generate DSRs and NLPs were conducted in the past years. Except the most energetic DSR obtained by Semaan *et al.* with 10 μJ single-pulse energy, most generated NLPs and DSRs from this configuration had low single-pulse power at nJ to hundreds nJ level such as a 140 nJ DSR by Mei *et al.* and a 91 nJ NLP by Chowdhury, *et al.* [16]–[18]. As the appearance of Raman component requires higher pulse power, only a few researches reported Raman in spectrum of DSR or NLP such as the Raman induced NLP by J. Liu, *et al.* [1]. Different from previous studies, we concentrate on investigating pulse dynamics at high power level by constructing the cavity mostly in 10 μm-core-diameter large-mode-area fiber. Moreover, obvious Raman peaks in pulse spectra of both NLP and DSR are obtained, which enrich study in this less concerned aspect.

Depending on the property of dual-pump figure-eight cavity, the saturation power changes with pump power intercoupling and polarization states controlling, thus providing an ideal platform for both NLPs and DSRs to evolve into versatile patterns. Two interesting phenomena are discovered in this experiment. One is that the output spectra consisting of a main peak and a Raman stokes peak. The central wavelength of the spectrum of the main peak can be tuned from 1075 to 1097 nm. The other is that the produced NLP presents an h-shaped profile before splitting while becomes square or h-shaped in different multiple states. A detailed description of the dual-pump figure-eight laser setup is provided in Section 2. Section 3 and 4 focus on the characteristics of multiple DSR pulses and NLP pulses respectively while conclusions will be drawn in Section 5.

2. Experimental Setup and Operation Principle

The experimental set-up as shown in Fig. 1, consists of a unidirectional loop and a NALM, which are connected by a 50% fiber coupler (OC2). Using 976/1030 nm pump-signal combiners, two pieces of 2 m YDF are cladding-pumped by two laser diodes (LD1 and LD2) with power range of around 25 W and 8 W separately. The circulator (CIR) acts as an isolator and an output coupler at the same time. The pulse output power is measured from the reflection port of the circulator. Three 1‰ couplers (MP1, MP2, MP3) are placed after the circulator and the NALM for pulse detection. The RF spectrum, optical spectrum and temporal pulse train are measured simultaneously from MP1, MP2 and MP3. The polarization controller (PC) used in this work is fiber squeezing one to help to adjust the polarization state. The pigtails of all components, the ytterbium-doped fiber (YDF) and passive fibers are in all 10 μm-core-diameter large-mode-area except for a length of 4.5 m 6

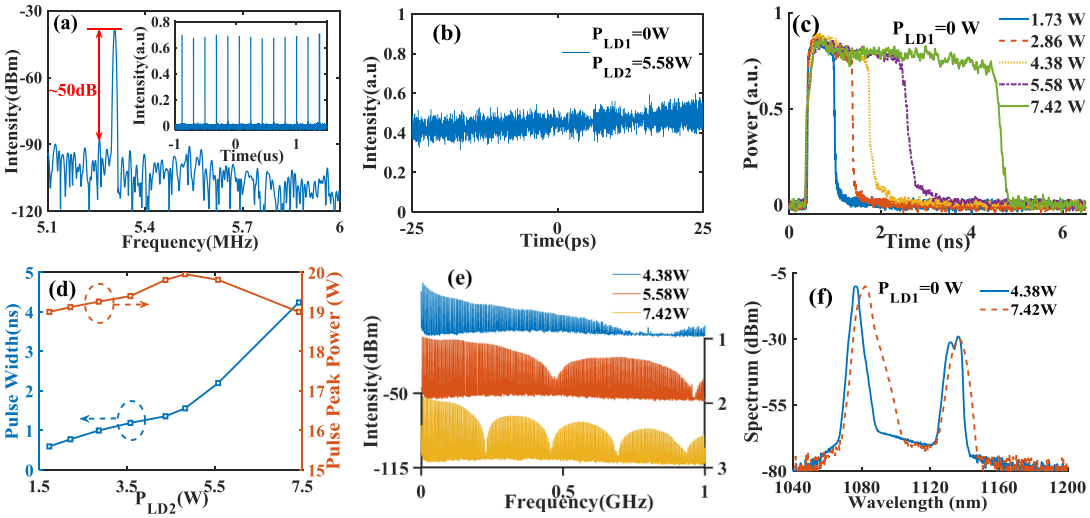

Fig. 2. The evolution of a DSR pulse with increasing pump power of LD2 when PLD1 is fixed at 0 W. (a) Single RF spectra. Inset: DSR pulse train. (b) Autocorrelation trace of the pulse. (c) Pulse widths of 0.6, 1, 1.36, 2.2 and 4.24 ns at LD2 powers of 1.73, 2.86, 4.38, 5.58 and 7.42 W, respectively. (d) Pulse peak power and width variation with LD2 power. (e) RF spectrum evolution as the increasing of power of LD2. (f) Pulse spectra at LD2 powers of 4.38 and 7.42 W.

μm-core-diameter single-mode-fiber in the NALM. The 4.5 m SMF adds to the cavity dispersion and nonlinearity thus makes a contribution to pulse breaking [19]. The total cavity length is about 35.7 m with a net dispersion of $\sim$0.72 ps^2. The dual-pump figure-eight cavity offers great flexibility in varying the saturable absorber properties such as the saturation power and modulation depth. Thus, adjusting the PC and power of two the LDs facilitates different pulse dynamics. In this way, NLP and DSR pulses can be switchable generated and involve into versatile patterns.

3. Dual-Pulses and Harmonic Patterns of DSR

Fixing power of LD1 to 0 W, when the power of LD2 exceeds a threshold of 1.73 W, a self-starting square pulse train of a repetition rate of $\sim$5.3 MHz could be easily observed. Fig. 2 depicts the characteristics of the DSR pulses. Once mode-locked, the laser produces a stable train of pulses with an interval of $\sim$188 ns as plotted in the inset of Fig. 2(a). The signal-to-noise ratio is 50 dB, indicating good temporal stability. The corresponding auto-correlation trace does not show any pulse or spike over a 50 ps window, suggesting that the pulse is free of any sub-structures. Pulse width variation with increasing pump power is shown in Fig. 2(c) which is also a signature attribute of DSR pulses. The graphs depicted in Fig. 2(d) show that the calculated pulse peak power keeps almost constant at 19$\sim$20 W with the increase of the LD2 power from $\sim$1.7 to $\sim$7.5 W when LD1 is fixed at 0 W, caused by the peak power clamping effect. Meanwhile, the pulse width widens from $\sim$0.6 to $\sim$4.24 ns. Note that the pulse top is not so flat, which is similar with those observed in some cavity configurations possibly because of gain competition [7], [9].

The modulation frequencies of three RF spectral distributions in Fig. 2(e) equal to the reciprocal of the native DSR pulse duration. Fig. 2(f) shows the optical spectrum trace of the generated square pulses under 4.38 and 7.42 W of power of LD2 in a fixed 0-W LD1. The spectrum consists of two peaks where the first peak is centered around 1080 nm with a triangular shape and the second peak is centered around 1135 nm. The spectral distance between the two central wavelengths remains at $\sim$55 nm, corresponding to the distance of Raman stokes line. The spectrum is largely broadened through the stimulated Raman scattering effect resulting from the high nonlinearity in the cavity. Along with the increase of LD2 power, central wavelengths of the two peaks shift towards the longer wavelength. Without employing any tunable wavelength-selected filter, the central wavelength of

the main peak can shift from 1075 to 1097 nm by adjusting the PC and manipulating the pump powers. This phenomenon had been reported and discussed in ref [20], in which it was explained by the birefringence-induced filtering effect. Although the fibers used in this experiment are all not polarization maintaining fibers, they could have weak birefringence due to slight imperfections during the fabrication process and the fiber winding. The ring structure of the fiber laser can be equivalent to a Lyot birefringence filter consisting of a length of birefringence fiber and two polarizers at both ends. Thus, the intracavity-birefringence-induced filter applies an amplitude transmission of which the transmission peak positions are related to the rotation of the PC [21]–[23]. Overall, up to 0.43-W average power and 81-nJ single pulse energy, undivided DSR pulses are generated with continuously tunable widths from 600 ps to 4.24 ns.

When LD1 is off in generating DSR pulse, the 10 μm-core-diameter large-mode-area YDF is not pumped, thus will be lossy to the signal [24]. Though unpumped YDF can act as saturable absorber that might cause Q-switching, the low absorption and slow switching time of YDF make it difficult to generate energetic pulses. Generally, the Q-switching pulses possess narrow 3-dB spectral width less than 1 nm and long pulse durations up to hundreds of ns or μs in experiment [25], [26]. Considering both the optical spectrum and real-time pulse profiles, there is no appearance of Q-switching which may result from the following reasons: the length of YDF inside NALM in our cavity is too long and the pump power is not strong enough to make the YDF bleach. Carefully adjusting the PC and enlarging the power of LD1, aiming for changing the nonlinearity parameters of the cavity, harmonic DSR and dual-pulses DSR are generated. The fundamental, 2nd, 3rd and 5th order DSR pulses are achieved as from the pulse trains shown in Fig. 3(a–d).

Apart from harmonic DSR, dual-pulse DSRs in fundamental and 2nd repetition rates are available under different pump powers as Fig. 3(e) and (f) shows. The interval between the sub pulses of the dual-pulse bunch decreases from fundamental to 2nd order repetition rate. Fig. 3(g) demonstrates the spectra under two harmonic DSR and two dual-pulse DSR states. The main peak of the spectra of the harmonic DSR centered at 1080 nm while that of the dual-pulse DSR centered at around 1075nm. According to the spectra distribution, it seems that harmonic DSR pulses are under one polarization state while dual-pulse DSR pulse are under another polarization state. Seen from Fig. 3(g), excited Raman stokes wavelength enlarges its intensity in (e)(f) compared with (c)(d), accompanying with the increase of pulse peak power after breaking to dual-pulse DSR states. Two typical RF spectra of harmonic and dual-pulse DSR is given in Fig. 3(h). The modulation frequency of 49 MHz corresponding to the intra-pulse separation of 20.4 ns as in Fig. 3(e). As the pulse width in Fig. 3(b) is less than 1 ns, corresponding RF spectra over 1 GHz decays smoothly without a modulation frequency. A bandpass filter (BPF) with a cutoff wavelength at 1100 nm is placed at the output to pass the wavelength component less than 1100nm. Fig. 3(i) and (j) show the spectra and pulse train of dual-pulse DSR pulse with and without the BPF. The excited Raman component is separated to the reflect port. The reflected spectrum is deliberately paralleled moved up by 22 dB as indicated in Fig. 3(i). In this way, it is clear to see that the suppression ratio of the bandpass filter is higher than 25 dB. The intensity and width of dual-pulse DSR from reflect and pass port remains nearly identical. Also, the vertical and horizontal polarized pulse components possess the same spectra and pulse intensities when connecting a polarization beam splitter at the output port. Thus, the DSRs break both different polarization states and wavelengths.

4. Versatile Patterns of NLP

Enlarging power of LD1 and adjusting PC, h-shaped NLP pulses are generated as displayed in Fig. 4.

As could be seen, each pulse exhibits a sharp leading peak and a following flat trailing portion, which is called the h-shaped pulse recently. This new type of pulse is experimentally observed and theoretically confirmed to share similar features as square pulse and achieve high pulse energy [9], [10]. The reported splitting pulses of the h-shaped pulse remain h-shaped and still increase with pumping power [27]. One possible mechanism for the formation of h-shaped pulse is that the pulse envelope contains an unclamped portion which is different from typical NLP pulses that are com-

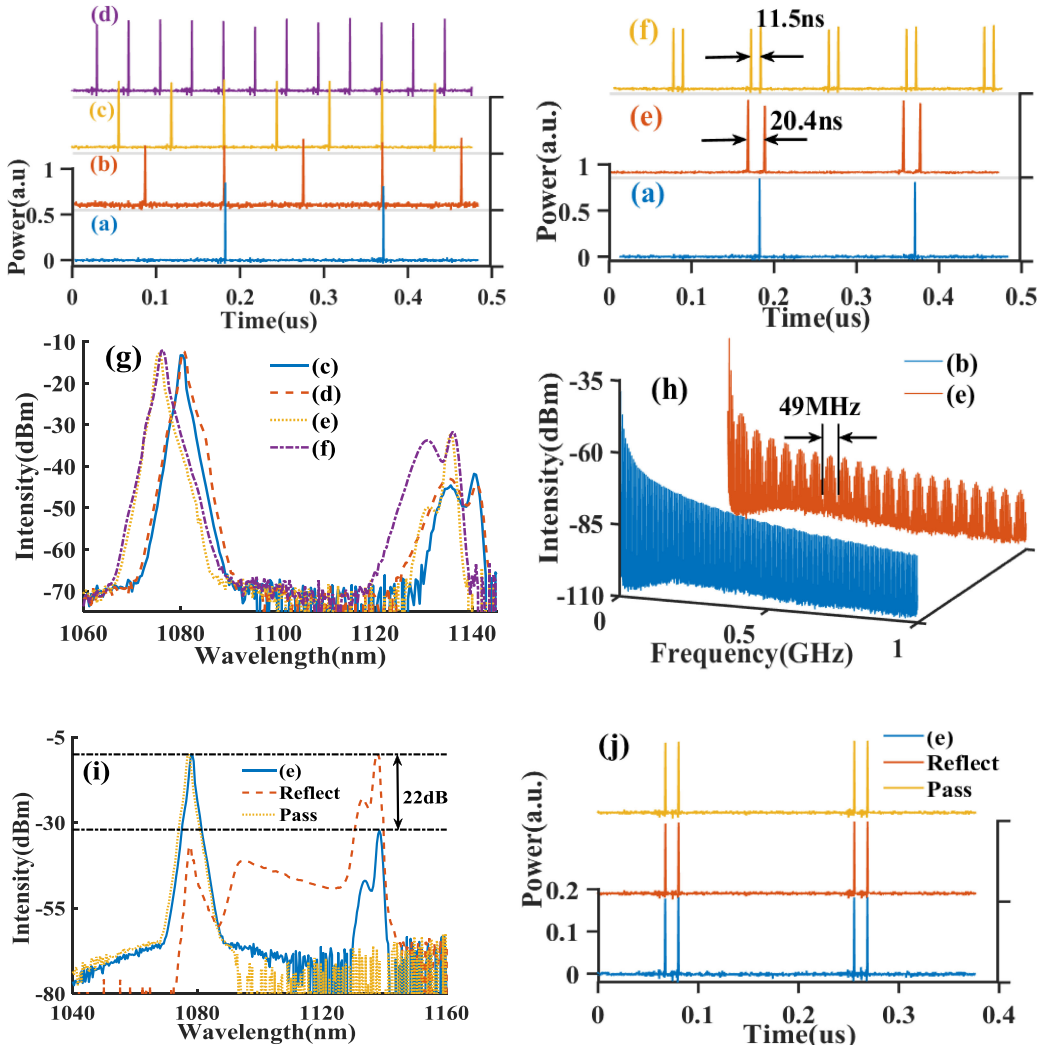

Fig. 3. Characteristics of harmonic DSR pulses. (a)–(d) Pulse trains of fundamental, 2nd, 3rd and 5th order DSR pulses. (e), (f) Dual-pulse DSR trains in fundamental and 2nd order. (g) Spectra of harmonic DSR pulses. (h) Two RF spectrum with 1GHz span and 5 kHz RBW. (i) Spectra (j) pulse train before and after bandpass filter of dual-pulse DSR pulse.

pletely clamped [10]. With increasing LD2 power from 0.78 to 7.18 W when PLD1 is fixed at 1.6 W, single NLP pulse extends the trailing part with a pulse duration from ~600 ps to ~3 ns as shown in Fig. 4(a) without pulse breaking, which is similar to the temporal characteristics of pulse working in a typical DSR regime. When PLD2 enlarges from 5.18 to 7.18 W, both the leading and trailing intensities increase. It seems that high pump power further induces asymmetry of the intensity distribution inside the pulse, just like the phenomenon reported in ref [10], [27]. Fig. 4(b) shows that corresponding pulse spectra intensity and 3-dB spectral width enlarge with the increase of PLD2. Meanwhile the stokes wavelength intensity rises because wider pulse can convert more energy to the Raman component. As in Fig. 4(c), when fixing the power of LD2 and enlarging LD1, the pulse leading part varies distinguished accompanying with a slightly narrow in pulse width of trailing part. Corresponding 3-dB spectral width in Fig. 4(d) enlarges but overall spectral intensity declines. The suppression ratio between main peak and the stokes wavelength decreases from 17.5 to 13 dB when PLD1 enlarges from 0 to 3.34 W. The peaks demonstrated in the autocorrelation trace in Fig. 4(e) indicates the pulse is in NLP operation. Fig. 4(f)–(h) show the pulse trains of single-pulse,

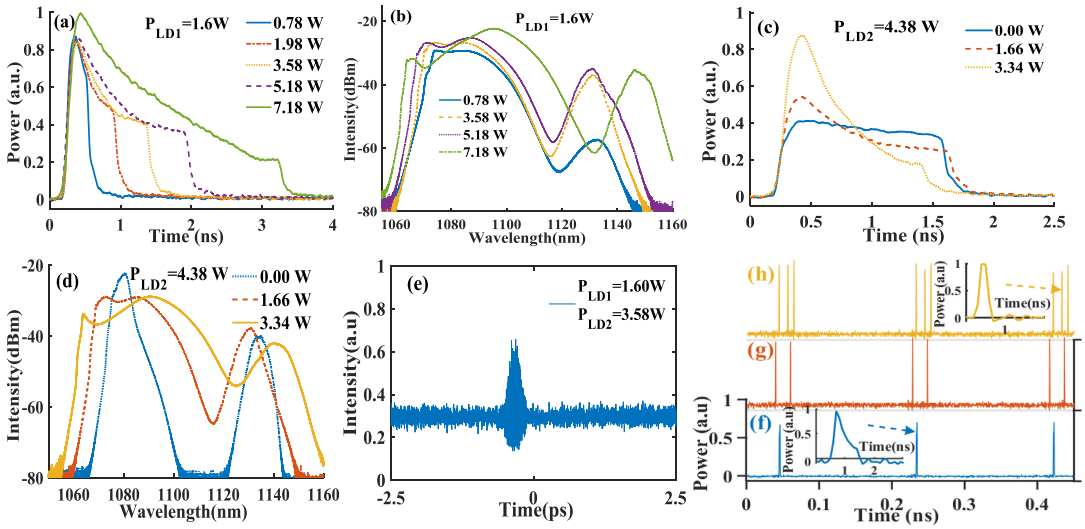

Fig. 4. Characteristics of single-pulse, dual-pulse and tri-pulse NLP. (a) Single NLP pulse temporal evolution and (b) spectra evolution with increasing pump power of LD2 when PLD1 is fixed at 1.6 W. (c) Single NLP pulse temporal evolution and (d) spectra evolution with increasing pump power of LD1 when PLD2 is fixed at 4.38 W. (e) Autocorrelation trace of the pulse. (f)–(h) Pulse trains of single-pulse, dual-pulse and tri-pulse NLP. Inset: Single pulses in detail.

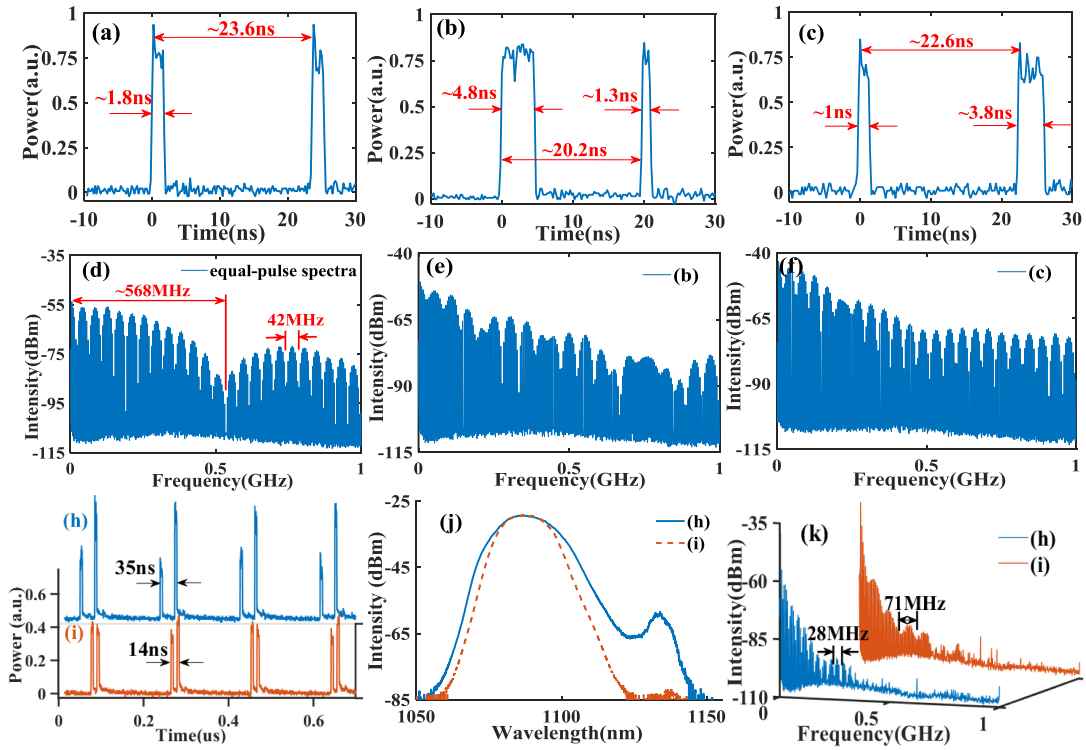

Fig. 5. Different types of dual-pulse NLP. Dual-pulse NLP with (a) equal pulse width and (b), (c) unequal pulse width. (d)–(f) RF spectra of (a)–(c). (h), (i) Pulse train, (j) spectra and (k) RF spectra of dual-pulse NLP with unequal pulse intensity.

dual-pulse and tri-pulse NLPs. Tri-pulse NLPs are always unevenly spaced. Noteworthy is that single-pulse NLP always appears as h-shaped before split but can become traditional square in dual-pulse or tri-pulse states as in the insets. However, single NLP would break into dual-pulse NLPs of several different patterns as shown in Fig. 5.

The dual-pulse NLPs appear when PLD1 and PLD2 vary in 3.4∼8.8 W and 4.4∼7.1 W. The dual-pulse NLPs presented in Fig. 5(a) have identical amplitude and pulse width around 1.8 ns with an intra-pulse separation of 23.6 ns. Fig. 5(d) shows the corresponding RF spectra where two modulations are found: one at 568 MHz corresponding to the pulse width of 1.8 ns and another at 42 MHz corresponding to the intra-pulse separation of 23.6 ns. Controlling the PC, dual-pulse NLPs of unequal pulse width can be generated as Fig. 5(b) and (c). They are square, not in the h-shaped. The width of the right pulse is not equal to the width of the left pulse. Moreover, the dual pulse intervals and each pulse width in dual-pulse NLP depend on polarization state. By squeezing the fiber using the PC, the polarization changes which influences the pulse interval and pulse width of dual-pulse NLP. Thus, it is reasonable to consider the pulse width of each pulse in dual-pulse NLP is polarization dependent. Resulting from unequal pulse width, corresponding RF spectra in Fig. 5(e) and (f) do not show fixed modulation period. Apart from dual-pulse NLP with non-uniform pulse width, there are dual-pulses with unequal intensity. As in Fig. 5(h), pulse in the trailing edge constantly possess higher intensity. In another polarization state in Fig. 5(i), the two pulses have little differences in intensity but periodic exchange the intensity relationship of each other. The intra-pulse separation also differs for state (h) and (i). Fig. 5(j) shows the spectra of dual-pulse NLPs in (h) and (i). One pulse in dual-pulse NLP in Fig. 5(h) possesses high intensity which contributes to the obvious Raman peak compared with spectra of (i). The spectra exhibit the same peak wavelength while the 3-dB bandwidth decreases obviously from state (h) to (i). Owing to the different dual-pulse intervals, the modulation period of RF spectra as marked in Fig. 5(k) enlarges from state (h) to (i).

5. Conclusion

In conclusion, we have experimentally investigated the switchable multipulse phenomenon of DSR and NLP in one cavity configuration. Multiple DSRs are same in amplitude, width and pulse intervals while dual-pulse and tri-pulse NLPs can be unevenly distributed with unequal pulse intensities. H-shaped pulses can break into square-wave NLPs instead of maintaining original shape. We consider this to be helpful in further enriching existing pulse dynamics and many applications may benefit from the diverse operations of this kind of dual-wavelength multi-state laser source.

References

[1] J. Liu *et al.*, "Generation and evolution of mode-locked noise-like square-wave pulses in a large-anomalous-dispersion Er-doped ring fiber laser," *Opt. Exp.*, vol. 23, pp. 6418–6427, 2015.
[2] A. Wang *et al.*, "Square-wave pulse with ultra-wide tuning range in a passively mode-locked fiber laser," *Opt. Lett.*, vol. 37, pp. 1334–1336, 2012.
[3] N. Akhmediev *et al.*, "Heat dissipative solitons in optical fibers," *Phys. Lett. A*, vol. 372, pp. 1531–1534, 2008.
[4] W. Chang *et al.*, "Dissipative soliton resonances," *Phys. Rev. A*, vol. 78, 2008, Art. no. 023830.
[5] A. Luo *et al.*, "Noise-like pulse trapping in a figure-eight fiber laser," *Opt. Exp.*, vol. 23, pp. 10421–10427, 2015.
[6] J. H. Cai *et al.*, "State distributions in two-dimensional parameter spaces of a nonlinear optical loop mirror-based, mode-locked, all-normal-dispersion fiber laser," *Opt. Exp.*, vol. 25, pp. 4414–4428, 2017.
[7] Z. Deng *et al.*, "Switchable generation of rectangular noise-like pulse and dissipative soliton resonance in a fiber laser," *Opt. Lett.*, vol. 42, pp. 4517–4520, 2017.
[8] Y. Lyu *et al.*, "Harmonic dissipative soliton resonance pulses in a fiber ring laser at different values of anomalous dispersion," *Photon. Res.*, vol. 5, pp. 612–616, 2017.
[9] S. Das Chowdhury *et al.*, "Multipulse dynamics of dissipative soliton resonance in an all-normal dispersion mode locked fiber laser," *J. Lightw. Technol*, vol. 36, pp. 5773–5779, 2018.
[10] J. Zhao *et al.*, "Cavity-birefringence-dependent h-shaped pulse generation in a thulium-holmium-doped fiber laser," *Opt. Lett.*, vol. 43, pp. 247–250, 2018.
[11] Y. Lyu *et al.*, "Multipulse dynamics under dissipative soliton resonance conditions," *Opt. Exp.*, vol. 25, pp. 13286–13295, 2017.
[12] A. Komarov *et al.*, "Competition and coexistence of ultrashort pulses in passive mode-locked lasers under dissipative-soliton-resonance conditions," *Phys. Rev. A*, vol. 87, pp. 5209–5214, 2013.

[13] C. Shang *et al.*, "Harmonic dissipative soliton resonance in an Yb-doped fiber laser," *J. Lightw. Technol*, vol. 36, pp. 4932–4935, 2018.
[14] Y. Huang *et al.*, "Versatile patterns of multiple rectangular noise-like pulses in a fiber laser," *Opt. Exp.*, vol. 24, pp. 7356–7363, 2016.
[15] O. Pottiez *et al.*, "Numerical study of multiple noise-like pulsing in a dispersion-managed figure-eight fibre laser," *Laser Phys.*, vol. 28, 2018, Art. no. 085108.
[16] G. Semaan *et al.*, "10uJ dissipative soliton resonance square pulse in a dual amplifier figure-of-eight double-clad Er:Yb mode-locked fiber laser," *Opt. Lett.*, vol. 41, pp. 4767–4770, 2016.
[17] S. D. Chowdhury *et al.*, "Diverse mode of operation of an all-normal-dispersion mode-locked fiber laser employing two nonlinear loop mirrors," *Appl. Opt.*, vol. 57, pp. 1225–1230, 2018.
[18] L. Mei *et al.*, "Width and amplitude tunable square-wave pulse in dual-pump passively mode-locked fiber laser," *Opt. Lett.*, vol. 39, pp. 3235–3237, 2014.
[19] D. Y. Tang *et al.*, "Mechanism of multisoliton formation and soliton energy quantization in passively mode-locked fiber lasers," *Phys. Rev. A*, vol. 72, 2005, Art. no. 043816.
[20] Y. Xu *et al.*, "Dissipative soliton resonance in a wavelength-tunable thulium-doped fiber laser with net-normal dispersion," *IEEE Photon. J.*, vol. 7, 2017, Art. no. 1502007.
[21] Z. R. Cai *et al.*, "A wide-band tunable femtosecond pulse fiber laser based on an intracavity-birefringence induced spectral filter," *Laser Phys.*, vol. 23, 2013, Art. no. 035107.
[22] S. J. Garth, "Birefringence in bent single-mode fibers," *J. Lightw. Technol.*, vol. 6, pp. 445–449, 1988.
[23] H. Xu, *et al.*, "Route to generate high-peak-power dissipative soliton resonance in a nonlinear amplifying loop mirror-based figure-eight laser," *Opt. Eng.*, vol. 58, pp. 036107-1–03617-7, 2019.
[24] S. W. Moore *et al.*, "400 μJ 79 ns amplified pulses from a Q-switched fiber laser using an Yb(3+)-doped fiber saturable absorber," *Opt. Exp.*, vol. 20, pp. 23778–23789, 2012.
[25] T. Tzong-Yow *et al.*, "Saturable absorber Q- and gain-switched all-Yb3+ all-fiber laser at 976 and 1064 nm," *Opt. Exp.*, vol. 18, pp. 23523–23528, 2010.
[26] B. Posada-Ramirez *et al.*, "All-fiber multi-wavelength passive *Q*-switched Er/Yb fiber laser based on a Tm-doped fiber saturable absorber," *Laser Phys.*, vol. 27, 2017, Art. no. 035103.
[27] J. Zhao *et al.*, "Tunable and switchable harmonic h-shaped pulse generation in a 3.03 km ultralong mode-locked thulium-doped fiber laser," *Photon. Res.*, vol. 7, pp. 332–340, 2019.